RADIOMETRIC RANGE IMAGE FILTERING FOR TIME-OF-FLIGHT CAMERAS

Faisal Mufti and Robert Mahony
Faculty of Engineering and Information Technology, ANU, Australia

Keywords: Time-of-flight camera (TOF), Reflectance model, Statistical analysis, Radiometric range criterion, Range filtering.

Abstract: Time-of-Flight (TOF) imaging devices provide distance measurements between the sensor and an observed target over a full image array at video frame rate. An essential step in the development of these devices is an understanding of the reliability of noisy range image data. This paper provides a unified frame work for TOF camera measurement and a radiometric reflectance model. A statistical analysis of the radiometric model is used to develop a range pixel reliability criterion to identify range errors. The radiometric model is verified using real data and the proposed range criterion is experimentally verified.

1 INTRODUCTION

In recent years, the demand for 3D vision systems has increased in a number of fields; such as; for example, detection and recognition (Fardi et al., 2006), 3D environment reconstruction (Kuhnert and Stommel, 2006) and tracking (Meier and Ade, 1997), etc. This has lead to increase effort in the development of range image technology and especially Time-of-Flight (TOF) cameras (Lange and Seitz, 2001). In general, 3D TOF cameras work on the principle of measuring time of flight of a modulated infrared light signal as phase offset after reflection and provide frame rate range and intensity data over a full image array at video frame rate (Kahlmann et al., 2007).

A key issue for TOF cameras is to evaluate the reliability of the range measurement from the received signal in the presence of noise (Moller et al., 2005). Noise due to systematic and statistical error is studied under various calibration methods based on experimental data acquired in a known environment (Kuhnert and Stommel, 2006). Kahlmann *et al.* (Kahlmann et al., 2006) characterized the cyclic deviation in distance measurement caused by uneven harmonics in modulation. Calibration techniques using lookup tables (LUT) for effect of temperature, reflectivity of the target and integration time on distance measurement have also been studied (Kahlmann et al., 2007; Radmer et al., 2008). Likewise, Lindner and Kolb (Lindner and Kolb, 2006) proposed depth error correction based on perspective calibration and linear adjustment but are constrained for high and low reflective surfaces that are closer to the camera or vice versa. These calibration methods, however, require a specific set of calibration experiments for each camera, and the resulting calibration minimization is an average approximation for each pixel.

The sensitivity of the distance measurement data obtained in a Time-of-Flight (TOF) camera is highly dependent on the signal-to-noise ratio (SNR) of active light received by the sensor. Noisy range values in a TOF camera are normally a result of a low integration time, a distant target or a signal received from low reflective surface in the camera. Attenuation due to distance is a result of classical inverse square law of signal attenuation and is straightforward to model. The link between integration time and noise of the received signal has been considered (Kahlmann et al., 2006). The effect of reflectivity on SNR, however, is more complex to model. Reflectivity is a parameter that depends on the observed scene (Lindner and Kolb, 2007) pixel by pixel as illustrated in Figure 1. Most real environment scenes consist of objects that can be modelled as Lambertian surfaces (Cook and Torrance, 1982). Since recovering reflectivity is a common problem in Shape From Shading (SFS), the reflectivity of Lambertian surfaces has been extensively studied (Zhang et al., 1999) in computer vision. Horn (Horn, 1977) approached this problem through the introduction of reflectance map. Techniques based on photometric stereo to recover surface albedo require multiple images or multiple sources to solve an

Mufti F. and Mahony R. (2010).
RADIOMETRIC RANGE IMAGE FILTERING FOR TIME-OF-FLIGHT CAMERAS.
In *Proceedings of the International Conference on Computer Vision Theory and Applications*, pages 143-152
DOI: 10.5220/0002819601430152

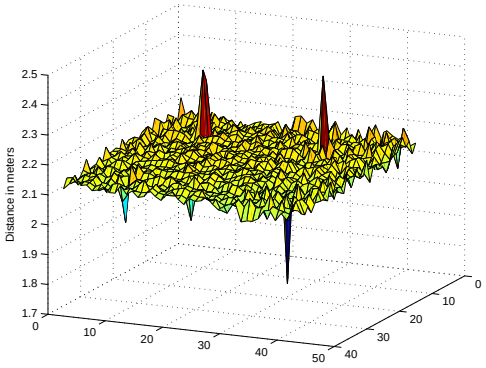

(a)

(b)

Figure 1: Range data (a) obtained for the PMD 3ks TOF camera imaging a flat board (b) pasted with nine low reflectivity patches. The SNR_{db} varies from 44.4db (forwhite board) to 7.3db (for the low reflective patches). The variation associated with low SNR is clearly visible in the range error seen in (a).

ill-conditioned inverse problem (Zhou et al., 2007). The complexity and the degree of error due to minimization algorithms (Zheng and Chellappa, 1991), and imaging conditions (Zhang et al., 1999) limits the applicability of reflectance modelling of environment in computer vision applications. Reliability of signal strength and range data in the presence of unknown reflectivity is a significant challenge for TOF cameras in real environments. To authors' knowledge there is little or no prior work to overcome TOF range measurement error due to signal strength variation, independent of scene reflectance.

This paper investigates the radiometric modelling of TOF measurements and background light sources by exploiting the dependencies between amplitude, intensity and range/phase measurements. We consider statistical noise model of TOF measurements, that along with radiometric properties of light sources, and a Lambertian reflectance model enable us derive a radiometric range model. Further in-depth statistical analysis of parameters of this model is used to formulate a radiometric range criterion. From this criterion we can effectively evaluate pixel-by-pixel reliability of range measurement in TOF cameras that is independent of scene reflectivity. For the purpose of this conference paper, we restrict our attention to the case of planar surfaces. The proposed reliability criterion helps in evaluating and filtering TOF range measurements under various SNR conditions, a key parameter for radiometric range criterion.

The paper is organized as follows: Section 2 describes TOF signal measurement, Section 3 provides statistical models for the measurements, Section 4 describes a reflectance model from TOF camera perspective and Section 5 presents a radiometric range model. In Section 6 we provide statistical analysis of radiometric range model, and then go on to propose a range pixel reliability criterion in Section 7. Section 8 presents experimental results of the implementation, and a short conclusion follows.

2 TIME-OF-FLIGHT SIGNAL MEASUREMENT

Time-of-Flight (TOF) sensors estimate distance to a target using the time of flight of a modulated infrared (IR) wave between the target and the camera. The sensor illuminates/irradiates the scene with a modulated signal of amplitude A (*exitance*) and receives back a signal (*radiosity*) after reflection from the scene with background signal offset I_o that includes non-modulated DC offset generated by TOF camera as well as ambient light reflected from the scene (see Figure 2).

There is a phase delay of the received modulated signal proportional to the ratio of range on speed of light of the observed point in the scene. The amplitude and phase of a modulated signal can be extracted by demodulating the incoming signal $A = A_i \cos(\omega t_i +$

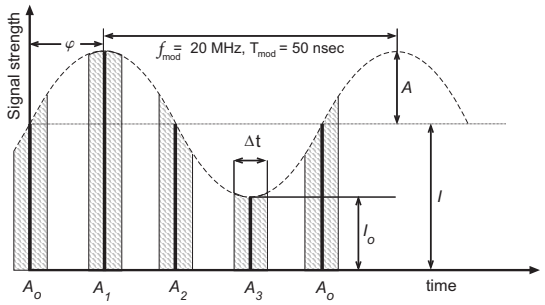

Figure 2: Received modulated signal in TOF camera. The signal of modulated frequency $f_{\text{mod}} = 20$Mhz with background illumination (exitance) I_o, is sampled four times A_o, A_1, A_2, A_3. These measurements are used to calculate amplitude A (1), phase φ (2) and intensity I (3).

$\varphi)+I$; $(t_i = i\cdot\frac{\pi}{2\omega}, i=0,\ldots 3)$ (see Figure 2) by synchronously sampling the received signal four times at quarter wavelength intervals of the modulated source frequency. The measured amplitude A, intensity I representing the gray scale image and the phase of the received signal are then respectively given by (Lange and Seitz, 2001)

$$A := \frac{\sqrt{(A_3-A_1)^2+(A_0-A_2)^2}}{2} \tag{1}$$

$$\varphi := \arctan\left(\frac{A_3-A_1}{A_0-A_2}\right). \tag{2}$$

$$I := \frac{A_0+A_1+A_2+A_3}{4}. \tag{3}$$

With known phase φ, modulation frequency f_{mod} and precise knowledge of speed of light c, it is possible to measure the un-ambiguous distance r from the camera as

$$r := \varpi\varphi; \qquad \text{where } \varpi = \frac{c}{4\pi f_{\text{mod}}}. \tag{4}$$

With a wavelength of $\lambda = \frac{1}{f_{\text{mod}}}$, this leads to a maximum possible unambiguous range of $\frac{\lambda}{2}$. For the PMD 3k-S TOF, the modulation frequency is 20MHz and the maximum unambigiuos range is 7.5m.

3 STATISTICAL NOISES MODELS OF THE MEASUREMENTS

It has been shown (Lange and Seitz, 2001) that photon shot noise effects the optical measurement process and is the major statistical noise process in TOF devices. In (Mufti and Mahony, 2009), statistical models for amplitude, phase and intensity were proposed that model the achievable signal-to-noise ratio (SNR) of the sensor device.

The statistical distribution of amplitude is a Rice distribution given by

$$\check{A} \sim \text{Rice}\left(A, \sqrt{I/2}\right), \tag{5}$$

where $\check{A}$ denote the actual measurement obtained by the TOF camera while A and I are the physical parameters of the model. The statistical distribution of phase $\check{\varphi}$ is given by

$$\begin{aligned}\Phi(\check{\varphi}|A,\varphi,\sqrt{I/2}) \;=\; & \frac{1}{2\pi}\exp\left(-\frac{A^2}{I}\right)\Big[1+\frac{A}{\sqrt{I}}\cos(\check{\varphi}-\varphi)\\ & (\sqrt{\pi})\exp\Big(\frac{A^2\cos^2(\check{\varphi}-\varphi)}{I}\Big)\\ & \Big\{1+\text{erf}\Big(\frac{A\cos(\check{\varphi}-\varphi)}{\sqrt{I}}\Big)\Big\}\Big],\end{aligned} \tag{6}$$

where erf(.) is the error function. Here Φ is a marginal distribution obtained by integrating over the joint distribution function of a complex version of the received signal (Bonny et al., 1996). The range measurement can be related to phase measurement based on the model (4) as

$$\check{r} = \varpi\check{\varphi}. \tag{7}$$

The statistical distribution for intensity is given by (Mufti and Mahony, 2009)

$$\check{I} \sim \mathcal{N}(I, I/4). \tag{8}$$

The measurements $\check{A},\check{I},\check{\varphi},\check{r}$ are thought of as the measured values of A, I, φ and r at pixel (x).

For a TOF camera a key performance parameter, SNR is defined as (Lange and Seitz, 2001; Büttgen et al., 2006; Mufti and Mahony, 2009)

$$\text{SNR} = \frac{\sqrt{2}A}{\sqrt{I}}. \tag{9}$$

In (Mufti and Mahony, 2009), the relationship of phase with SNR has been shown by noting the fact that although the phase distribution (6) is written with dependence on three parameters $(A,\varphi,\sqrt{I/2})$, in fact only the ratio, $\frac{A}{\sqrt{I/2}}$, appears on the right hand side in the definition of (6). Consequently the phase distribution can be re-written as

$$\check{\varphi} \sim \Phi\left(\check{\varphi}\left|\frac{A}{A},\varphi,\frac{\sqrt{I}}{\sqrt{2}A}\right.\right) = \Phi\left(\check{\varphi}\left|1,\varphi,\frac{1}{\text{SNR}}\right.\right). \tag{10}$$

The model for SNR is a generic model for TOF cameras (Büttgen et al., 2006). In practice manufacturers vary the configuration for customized designs to improve performance in ways that do not fundamentally change the physics of the model but leads to scaling effects that must be modelled. This process for raw measurements is discussed in (Luan, 2001; Mufti and Mahony, 2009) and is not further considered in this paper, although these effects must be understood to obtain experimental results.

We define a second key statistical factor for performance measurement in TOF camera as signal-to-offset ratio (SOR) of photon count. This ratio reflects the total offset in the received signal with respect to the amplitude of the modulated source and is given by

$$\begin{aligned}\text{SOR} \;&=\; \left(\frac{\text{received signal amplitude}}{\text{value of the background offset}}\right)\\ &=\; \left(\frac{A}{I_o}\right).\end{aligned} \tag{11}$$

4 REFLECTANCE MODEL

The active signal of a TOF camera can be used for measurement of amplitude A, intensity I, and range r. These measurement parameters are not independent but depend on the reflectance characteristics of the scene. In order to develop reliability criteria for TOF data it is necessary to provide background theory for a reflectance model for time-of-flight (TOF) camera and understand the signal behavior in a radiometric framework.

A reflectance model gives a relationship for light emitted and received between a source, a surface and the observer or the camera image plane. We consider a near-field IR point source for the camera's active LED array and a far-field source for background illumination.

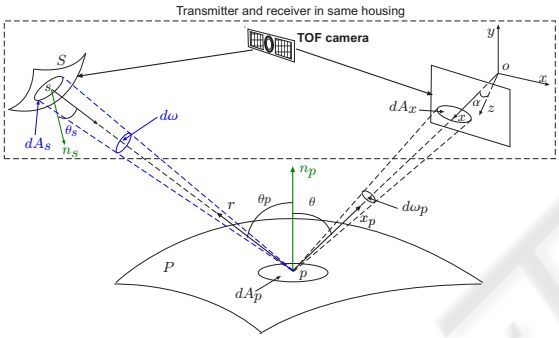

Figure 3: Geometry of reflectance model for Time-of-Camera. Note that although the source and receiver of a physical TOF camera are co-located, it is difficult to provide a visualization of this geometry. Here the source is shown separately to make is easier to see notation, however, in practice the directional vectors r and x_p are equal.

4.1 Reflectance Model for an IR Source of TOF Camera

The primary source of illumination in TOF cameras is an IR source that produces a modulated IR signal offset by a non-modulated DC signal. The reflectance model takes into account the modulated signal represented by $A(s)$ as well as the non-modulated DC signal represented by $I_c(s)$.

Modulated IR Source. Let P be a Lambertian surface in space with n_p the normal to the each point $p \in P$ on the surface as shown in Figure 3. Let a modulating IR point source S is irradiating the surface P then $d\omega$ denote the solid angle of dA_s seen from point p. Then

$$d\omega = \frac{\cos\theta_s dA_s}{r^2}, \tag{12}$$

where θ_s is the angle between the normal to the source point $s \in S$ and the ray of the modulated IR signal reaching point p, and r is the distance between source and the point p. Following the laws of radiometry (Sillion and Puech, 1994) the amplitude of total radiance $A(p)$ (called *radiosity*) leaving point p due to illumination by the modulated signal $A(s)$ is proportional to the *diffuse reflectance* or *albedo* $\rho(p)$ and the integral of irradiance over all the possible incoming directions in a hemisphere, Ω, scaled by the cosine of arrival angle θ_p (Ma et al., 2003) (p. 68)

$$A(p) = \int_\Omega \frac{1}{\pi}\rho(p)A(s)\cos\theta_p d\omega. \tag{13}$$

By substituting (12) into (13) and changing the domain of integration to the surface, S, of the source (Forsyth and Ponce, 2003) (p. 77), one has

$$A(p) = \int_S \frac{1}{\pi}\rho(p)\frac{A(s)\cos\theta_p\cos\theta_s dA_s}{r^2}. \tag{14}$$

An active TOF camera senses the received modulated IR signal within its field of view and all the points on surface illuminated by the camera can observe the same source. In the present analysis, the LED point sources of the camera are part of the compact IR array of the TOF camera, and can be approximated by a single virtual modulated point source (Forsyth and Ponce, 2003, p. 78) with the center of illumination aligned with the center of projection and the optical axis of the camera (Kuhnert and Stommel, 2006). In this case, the integration (14) can be re-written as a function of the exitance of a single point source as

$$A(p) := \frac{1}{\pi}\rho(p)\frac{A(s)\cos\theta_p\cos\theta_s}{r^2}. \tag{15}$$

Using the thin lens assumption, irradiance on an image plane can be expressed by measuring the radiosity along the direction x that depends on the geometry of the lens capturing the light (Ma et al., 2003, p. 48) as

$$A(x) = \Upsilon A(p). \tag{16}$$

Here Υ is the lens collection representing irradiance fall-off with cosine-fourth law (Horn, 1986) (p. 208) as

$$\Upsilon = \frac{\pi}{4}\left(\frac{d}{f'}\right)^2\cos^4\theta_x, \tag{17}$$

where d is the diameter of the lens, f' is the focal length of the lens and θ_x is the angle of the ray from the principle axis.

Non-modulated IR Source. The TOF camera IR source produces a DC signal from the same IR source LEDs. This signal will have the same reflectance model as has been derived for the modulated

IR source (see (15)). One has

$$I_c(p) := \frac{1}{\pi}\rho(p)\frac{I_c(s)\cos\theta_p\cos\theta_s}{r^2}, \qquad (18)$$

where the received signal $I_c(x)$ is given by

$$I_c(x) = \Upsilon I_c(p). \qquad (19)$$

The effect of this signal is an added offset to the modulated signal for better illumination of the scene.

4.2 Reflectance Model for Background Illumination

We also consider the background illumination of the scene due to ambient light in TOF camera. In computer vision (Alldrin et al., 2008) and computer graphics (Cook and Torrance, 1982), a single view point source of local shading model and an ambient illumination model is generally preferred and we would restrict our attention to these two models of background illumination.

Ambient Background Illumination. Consider an ambient background illumination of the scene i.e an illumination that is constant for the environment and produces a diffuse uniform lighting over the object (Foley et al., 1997) (p. 723). Let I_a be the intensity (called *exitance*) of the ambient illumination, then the received intensity $I_a(p)$ from a point p is expressed as

$$I_a(p) = \frac{1}{\pi}\rho(p)I_a, \qquad (20)$$

where ρ, is the *ambient reflection coefficient* of a surface. The irradiance on the image plane is given by

$$I_a(x) = \Upsilon I_a(p). \qquad (21)$$

Far Field Background Illumination. For real environments we also consider far-field point sources. For a point source that is far away as compared to the area of the target surface, the exitance does not depend on the distance from the source or the direction in which the light is emitted (Forsyth and Ponce, 2003) (p. 76).

The radiosity of point p due a point source $q \in Q$, defined as $I_b(p)$, can be obtained by integrating each of the sources as

$$I_b(p) = \frac{1}{\pi}\rho(p)\int_Q I_b(q)\cos\theta_q dA_Q, \qquad (22)$$

where θ_q is the angle between normal to the surface point p and the source point q, $\rho(p)$ is the surface albedo at point p and dA_Q is the infinitesimal area of a source Q. Considering a single IR far-field background point source of illumination, the radiosity perceived by TOF image plane due to this IR source is given as

$$I_b(x) = \Upsilon I_b(p). \qquad (23)$$

where

$$I_b(p) = \frac{1}{\pi}\rho(p)I_b(q)\cos\theta_q. \qquad (24)$$

5 RADIOMETRIC RANGE MODEL

In Section 4, we derived the reflectance model for the signal received by TOF camera. The perceived radiosity for each pixel x is highly dependent on the unknown diffuse reflectance $\rho(p)$ (see (15), (18), (20) and (24)). The value of this parameter ranges between 0 and 1. The received signal can have large fluctuations corresponding to a different reflectivity of different points p in the scene observed at pixel x. As a consequence, there is a significant deviation in statistical distribution of distance measurements for TOF camera for different reflective surfaces (Lindner and Kolb, 2007; Mufti and Mahony, 2009). The received signal obtained after reflection from object with very low reflectivity will lie in a region of low SNR. In 2D cameras the only available measurement is intensity and photometric stereo techniques are used to estimate reflectivity from multiple images or light orientations to solve the associated under-determined system. A TOF camera, however, measures amplitude, intensity and phase. Hence, it is possible to create a unified reflectance model based on all the available measurement parameters that is robust against limitation of unknown reflectivity.

From the basic principles of TOF camera signals shown in Figure 1, we know that the intensity component of TOF carries information for both, amplitude of the modulated signal and the background offset I_o. Thus, we can represent the mean offset represented by intensity of TOF cameras as

$$I := A + I_o. \qquad (25)$$

The background offset I_o is composed of DC offset due to TOF camera I_c and background illumination I_a and I_b depending upon the environment where TOF camera is operating. One has

$$I_o = I_c + I_a + I_b. \qquad (26)$$

Indexing the point p in the scene by the TOF receiving pixel x and dividing (25) by $A(x)$ and substituting (26), one obtains

$$\frac{I(x)}{A(x)} = 1 + \frac{I_c(x)}{A(x)} + \frac{I_a(x)}{A(x)} + \frac{I_b(x)}{A(x)}. \qquad (27)$$

Using the local shading model for IR signal and the background illumination of point sources (16), (19), (21) and (23), one can re-write (27) as

$$\frac{I(x)}{A(x)} = 1 + \frac{I_c(s)}{A(s)} + \frac{I_a r^2(x)}{A(s)\cos\theta_p \cos\theta_s} + \frac{I_b(q)\cos\theta_q r^2(x)}{A(s)\cos\theta_p\cos\theta_s}, \tag{28}$$

where $\theta_s := \theta_s(x)$ is a function of pixel.

The ratio of background ambient light I_a to modulated TOF IR source $A(s)$ can be defined as

$$\kappa_a := \frac{I_a}{A(s)}. \tag{29}$$

Observe that κ_a does not depend upon scene or camera geometry and hence is a constant parameter over the full image array. Similarly, define

$$\kappa_b := \frac{I_b(q)}{A(s)}, \tag{30}$$

as the ratio of far-field illumination and the TOF IR source. The parameter κ_b is once again a constant parameter independent of scene or pixel coordinates. Finally we define κ_c as the ratio of TOF non-modulated IR source $I_c(s)$ and TOF modulated IR source $A(s)$

$$\kappa_c := \frac{I_c(s)}{A(s)}, \tag{31}$$

Since the two sources of illumination originate from the same IR LED source, any surface in the scene will receive same amount of modulated and non-modulated TOF IR source due to identical angle of illumination. Thus we can redefine (31)

$$\kappa_c(x) := \frac{I_c(x)}{A(x)}. \tag{32}$$

where $\kappa_c(x)$ is function of a pixel $x \in \mathbb{R}^2$ and is a camera based pixel parameter for an entire image. In theory $\kappa_c(x) = \kappa_c$ for all x that varies with the integration time. However, in practice slight variation in the CMOS circuitry causes pixel variation in $\kappa_c(x)$ and is modelled using calibration techniques documented in Section 6.

The parameters (κ_a, κ_b) are constant over the image plane. For any surface patch[1], it is possible to numerically compute an estimate of the angle $\theta_p(x)$ from the set of range measurements $r(x_i)$ associated with that patch based on an estimate of the normal vector to the surface (Pulli and Pietikainen, 1993; Klasing et al., 2009; Ye and Hedge, 2009). For the far field source we add two parameters $(\theta_{az}, \theta_{el})$ that describe its azimuth and elevation with respect to the camera frame. Given the estimate θ_{az}, θ_{el} then it is also straightforward to compute $\theta_q(x)$. We think of these angles as functions of range data from pixels corresponding to a local surface around a point in the image. That is, denoting the local neighbourhood of x by $\{x_i\}_{i=1}^n$ used in the calculation of normal to x, one has

$$\theta_p(x) := F_{\theta_p}[r(x_1), \cdots, r(x_n)] \tag{33}$$

$$\theta_q(x) := F_{\theta_q}[r(x_1), \cdots, r(x_n), \theta_{az}, \theta_{el}]. \tag{34}$$

Although the present spatial resolution of TOF cameras have significant limitations, it is clear that future technology will lead to TOF cameras with potentially much higher resolution, making this process highly effective.

Thus, using the parameters $(\kappa_a, \kappa_b, \kappa_c, \theta_{az}, \theta_{el})$ of sources one obtains a radiometric relationship as

$$\boxed{\frac{I(x)}{A(x)} = 1 + \kappa_c(x) + \kappa_a \frac{r^2(x)}{\cos\theta_p \cos\theta_s} + \kappa_b \frac{\cos\theta_q r^2(x)}{\cos\theta_p \cos\theta_s}.} \tag{35}$$

The above radiometric relationship is independent of reflectivity $\rho(p)$ and relate the measurable variables A, I, r to constant parameters $\kappa_a, \kappa_b, \kappa_c$ and θ_{az}, θ_{el}.

5.1 Radiometric Range Model for Planar Case

In this paper, we will only consider the case of radiometric range model for planar surfaces using (35). Consider the case of a single planar surface in the field of view of TOF camera. Over this single surface it can be easily seen that θ_q is constant while θ_p is nearly constant for a small field of view of TOF optical sensor over the surface. As a result several parameters can be combined into a single constant. We propose an approximate model

$$\frac{I(x)}{A(x)} = 1 + \kappa_c(x) + \kappa_o \frac{r^2(x)}{\cos\theta_s}, \tag{36}$$

where

$$\kappa_o := \frac{\kappa_a}{\cos\theta_p} + \frac{\kappa_b \cos\theta_q}{\cos\theta_p} = \text{constant}. \tag{37}$$

As a consequence of (37), a pixel measurement of κ_o is given by

$$\kappa_o(x) = \left(\frac{I(x)}{A(x)} - \kappa_c(x) - 1\right)\frac{\cos\theta_s}{r^2(x)}. \tag{38}$$

We will use $\kappa_o(x)$ as a radiometric criterion for range reliability.

In practice the measurement of $\kappa_o(x)$ is a noisy process due to noise in the statistical distribution of measurement obtained. In the next section we provide a detailed analysis of statistical distributions of $\kappa_o(x)$ and parameters associated with it due to the noise in the measurement process.

[1]The surface patch must be sufficiently large to be imaged by a small window of pixels.

6 STATISTICAL DISTRIBUTION OF $\check{\kappa}_o(x)$

We have seen that κ_o is a function of constant sources (camera source and the background source of illumination) that cannot be directly measured in practice. The relationship (38) provides a mean to measure κ_o in practice. A statistical analysis of the measurement of $\kappa_o(x)$ in this section will provide a significant insight into radiometric range model for the planar case.

Consider a pixel x in the TOF image array and define the measurement $\check{\kappa}_o(x)$ as

$$\check{\kappa}_o(x) := \left(\frac{\check{I}}{\check{A}} - \hat{\kappa}_c - 1\right)\frac{\cos\theta_s}{\check{r}^2}, \tag{39}$$

where $\hat{\kappa}_c$ is an estimate of camera based parameter for an entire image. A $\check{\kappa}_o(x)$ is complex statistical distribution composed of ratio of different distribution and as such a closed form analytic solution is not possible. However, based on the distributions of measurements $\check{A},\check{I},\check{r}$ and the estimate of $\hat{\kappa}_c$, we can represent the statistical distribution of $\check{\kappa}_o(x)$ in terms of independent parameters. The statistical distributions of $\check{A},\check{I}$ and $\check{r}$ have been discussed in Section 3.

The ratio of modulated and non-modulated IR source of TOF camera, $\kappa_c(x)$, is fixed for each pixel and is determined as a pre-processing step in TOF radiometric range estimation. The estimation of $\kappa_c(x)$ defined as $\hat{\kappa}_c$ is a measurement process over a large data set. For sufficient samples central limit theorem ensures that,

$$\hat{\kappa}_c \sim \mathcal{N}\left(\kappa_c(x), \frac{1}{N}\sigma^2[\kappa_c(x)]\right). \tag{40}$$

By knowing the distribution of dependent parameters we can now show that $\check{\kappa}_o(x)$ is sampled from a distribution with three pixel based independent parameters SNR, SOR and κ_o. The two parameters κ_c and θ_s are camera parameters that can be calibrated in the initial setup of the camera and are not considered parameters of the distribution.

Lemma 1: $\check{\kappa}_o(x)$ **Distribution Parameters.** *Assume the camera parameters $\kappa_c(x)$ and θ_s are known and $\check{A}(x),\check{r}(x),\check{I}(x)$ are given by (5),(7) and (8). Then the measurement*

$$\check{\kappa}_o(x) = \left(\frac{\check{I}(x)}{\check{A}(x)} - \kappa_c(x) - 1\right)\frac{\cos\theta_s}{\check{r}^2(x)}, \tag{41}$$

can be modelled as a random variable with distribution depending on three independent parameters SNR (9), SOR (11) and κ_o (37).

Proof: Recall that $A(x),I(x)$ and $r(x)$ are the underlying radiometric parameters of the ideal received signal based on noise free radiometric model. For ease of notation we drop the (x) dependence such that $A = A(x), I = I(x)$. Using the definition of SOR (11) and (26), one can write

$$\frac{1}{\text{SOR}} = \frac{I_a + I_b + I_c}{A}. \tag{42}$$

Using (37), one has

$$\kappa_o = \frac{1}{A(s)\cos\theta_p}\left(I_a + I_b(q)\cos\theta_q\right). \tag{43}$$

Define new scaled measurement $\bar{A} := \check{A}/A$ and $\bar{I} := \check{I}/A$ then it is straight forward to verify from (5) and (8) that

$$\bar{A} = \frac{\check{A}}{A} \sim \text{Rice}\left(\frac{A}{A}, \frac{\sqrt{I}}{\sqrt{2}A}\right) = \text{Rice}\left(1, \frac{1}{\text{SNR}}\right) \tag{44}$$

$$\bar{I} = \frac{\check{I}}{A} \sim \mathcal{N}\left(\frac{I_o + A}{A}, \frac{I}{4A^2}\right) = \mathcal{N}\left(\frac{1+\text{SOR}}{\text{SOR}}, \frac{1}{2\cdot\text{SNR}^2}\right) \tag{45}$$

Using the radiometric model (16) for the true range r, one has

$$\begin{aligned} r^2 &= \frac{\Upsilon\rho(p)}{\pi}\frac{A(s)\cos\theta_p\cos\theta_s}{A} \\ &= \frac{\Upsilon\rho(p)}{\pi}\frac{A(s)\cos\theta_p\cos\theta_s}{A}\frac{(I_a + I_b(q)\cos\theta_q)}{(I_a + I_b(q)\cos\theta_q)} \\ &= \cos\theta_s\left(\frac{A(s)\cos\theta_p}{I_a + I_b(q)\cos\theta_q}\right)\frac{I_a + I_b}{A}. \end{aligned} \tag{46}$$

Substituting (42) and (43), we obtain

$$r^2 = \frac{\cos\theta_s}{\kappa_o}\left(\frac{1}{\text{SOR}} - \kappa_c\right). \tag{47}$$

As a consequence of (4) one can write the true phase as

$$\varphi := \frac{1}{\varpi}\sqrt{\frac{\cos\theta_s}{\kappa_o}\left(\frac{1}{\text{SOR}} - \kappa_c\right)} \tag{48}$$

Hence, using (7) and (10) we have shown

$$\check{r} \sim \frac{1}{\varpi}\Phi\left(\frac{\check{r}}{\varpi}\middle| 1, \sqrt{\frac{\cos\theta_s}{\kappa_o}\left[\frac{1}{\text{SOR}} - \kappa_c\right]}, \frac{1}{\text{SNR}}\right). \tag{49}$$

This shows that $\check{r}$ is a random variable with parameters SNR, SOR and κ_o. From (41), using (44),(45) and (49) one has

$$\check{\kappa}_o(x) = \left(\frac{\bar{I}}{\bar{A}} - \kappa_c - 1\right)\frac{\cos\theta_s}{\check{r}^2}. \tag{50}$$

Thus, the expression for $\check{\kappa}_o(x)$ is a function of random variables $\bar{A},\bar{I}$ and $\check{r}$. The random variables depend in

turn on the parameters SNR, SOR and κ_o (44),(45) and (49). Consequently, $\check{\kappa}_o(x)$ is a random variable depending on parameters SNR, SOR and κ_o.
■

Let f_x denote the distribution function for $\check{\kappa}_o(x)$. That is

$$\check{\kappa}_o(x) \sim f_x(\check{\kappa}_o(x)|\text{SNR},\text{SOR},\kappa_o). \quad (51)$$

The SNR is the dominant parameter of $\check{\kappa}_o(x)$ distribution due to the shot noise associated with Poisson arrival process of photons of TOF signal and effects the spread or tail of $\check{\kappa}_o(x)$ distribution. The parameters SOR and κ_o effect the mean value of the distribution.

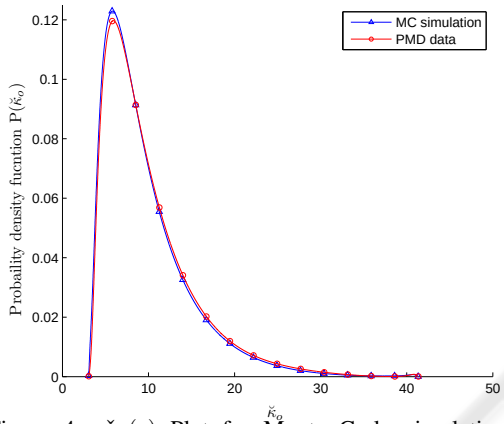

Figure 4: $\check{\kappa}_o(x)$ Plot for Monte Carlo simulation and real data from PMD camera (SNR_{db}=12.14db, SOR_{db}=-38.61db, κ_o=8.39).

It appears to be extremely difficult to derive an analytic expression for the distribution of $\check{\kappa}_o(x)$. We verify the model using Mote Carlo simulation with model parameters A, I and φ to plot $\check{\kappa}_o(x)$ distributions (with parameters SNR, SOR, and κ_o). A low SNR case is plotted in Figure 4. The measured range variation for this case is between 1.95m to 3.82m. The simulation data matches with the experimental data, confirming the validity of the proposed model parameters.

7 RADIOMETRIC RANGE CRITERION FOR PIXEL RELIABILITY

In this Section, we propose an algorithm for radiometric range filtering. The statistical analysis of $\check{\kappa}_o(x)$ distribution (51) lead us to formulate a reliability criteria based on a statistical test for $\check{\kappa}_o(x)$. That is given estimates $\widehat{\text{SNR}}(x), \widehat{\text{SOR}}(x)$ and $\hat{\kappa}_o(x)$ of parameters SNR, SOR and κ_o at pixel x, let $\alpha > 0$ significance level, choose $m(x)$ such that

$$P_{f_x}\left[(\check{\kappa}_o(x) < m(x))|\widehat{\text{SNR}}(x), \widehat{\text{SOR}}(x), \hat{\kappa}_o(x)\right] = \alpha, \quad (52)$$

where

$$\int_{m(x)}^{\infty} f_x[\check{\kappa}|\widehat{\text{SNR}}(x), \widehat{\text{SOR}}(x), \hat{\kappa}_o(x)]d\check{\kappa} = \alpha. \quad (53)$$

Then, $\check{\kappa}_o(x)$ is accepted if $\check{\kappa}_o(x) < m(x)$.

Consider a single frame of data and note that the estimates of $\widehat{\text{SNR}}(x)$ and $\widehat{\text{SOR}}(x)$ can be computed pixel-by-pixel as

$$\widehat{\text{SNR}}(x) = \frac{\sqrt{2}\check{A}}{\sqrt{\check{I}}}; \qquad \widehat{\text{SOR}}(x) = \frac{\check{A}}{\check{I}_o}, \quad (54)$$

where $\check{I}_o$ is the measured background offset. In addition, it is necessary to compute the estimate of $\hat{\kappa}_o(x)$ at pixel x. Based on the assumption of a flat surface the true value of $\kappa_o(x)$ will only deviate from a constant due to viewing angle of the surface θ_p. This angle is approximately constant for small field of view cameras. Therefore, we approximate $\kappa_o(x) \approx \kappa_o$ over pixels of the planar surface. Moreover, we find in practice that the SNR and SOR over a single planar surface are comparable and we can make an estimate $\hat{\kappa}_o$ of κ_o based on average statistics of this data set.

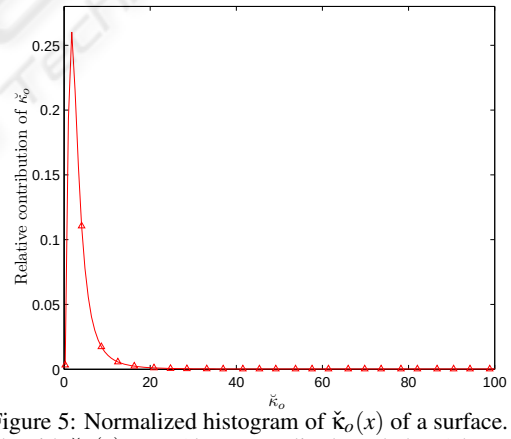

Figure 5: Normalized histogram of $\check{\kappa}_o(x)$ of a surface. Pixels with $\check{\kappa}_o(x) \to \infty$ (due to amplitude and phase) have been scaled down to finite values.

A typical normalized histogram of $\check{\kappa}_o(x)$ for a single frame of a planar surface is shown in Figure 5. The heavy tail is associated with noisy data. We propose a pragmatic approach (a practical estimator) for κ_o using the harmonic mean

$$\hat{\kappa}_o = \frac{n}{\sum_i^n 1/\check{\kappa}_{o(x)_i}} \quad (55)$$

It is reasonable to use the harmonic mean (Bodek, 1974) due to the fact that each individual $\check{\kappa}_o(x)$ is a

ratio distribution with different SNRs of the received signal measured in TOF camera and the error measurements of $\check{\kappa}_o(x)$ in denominator being greater than that of a numerator.

The statistical test (52) can be applied to all pixels drawn from a planar surface. The parameters $\widehat{\mathrm{SNR}}, \widehat{\mathrm{SOR}}, \hat{\kappa}_o$ estimated from the same data that is then used in the test, however, the slight dependence introduced is not believed to effect the overall validity of the test significantly if there are enough pixels in the given observed surface (typically a 5×5) patch.

8 EXPERIMENTS AND RESULTS

We perform experiments in an indoor environment where a TOF camera is placed conveniently at a distance of 3 meters from a flat white board while the wall is about 6 meters from the camera as illustrated in Figure 6. In addition there are various other objects and lab equipment within the field of view of camera. These objects offer different reflectivity and provide a wide variety of characteristics for the experiments undertaken. Our PMD 3k-S(PMD, 2002) TOF camera provides 48×64 pixel resolution with a field of view of $33.4^\circ \times 43.6^\circ$.

Figure 6: Picture taken from a normal 2D camera for a tripod mounted TOF camera setup.

The algorithm is applied to an entire frame and a $\check{\kappa}_o(x)$ distribution is plotted for a planar surface (a wall) (see Figure 5). The final range data as a function of $\check{\kappa}_o(x)$ is obtained after applying the range image filtering criterion (52) to the entire frame including planar surface as shown in Figure 8.

The final6data after filtering is consistent with a reliable measurement of range values. It is quite clear that $\check{\kappa}_o(x)$ value is almost consistent for the entire range (0-7.5 meters) of the camera with noisy data pixels (see Figure 7) showing a variation in $\check{\kappa}_o(x)$ values as shown in Figure 8. The algorithm is neither effected by the distance of the object from the camera (within camera range) nor the reflectively/surface

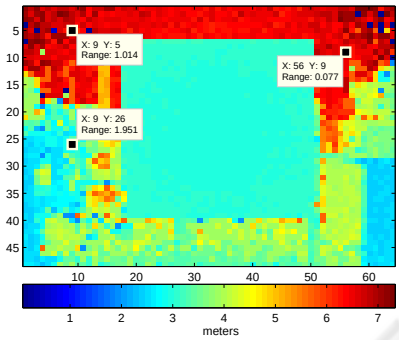

Figure 7: Range image plot of a PMD TOF camera with three marked noisy (in-correct) range pixels.

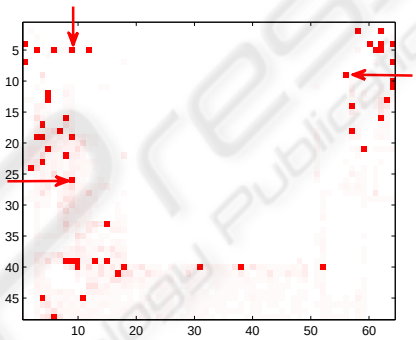

Figure 8: Filtered $\check{\kappa}_o(x)$ plot with regions of consistent $\check{\kappa}_o$ and noisy pixels shown in red color. Three pixels marked with arrows relate to marked noisy range pixels in Figure 7.

texture for wide range of integration times and SNR conditions compared to other image algorithms that are otherwise susceptible to surface conditions. It has been observed that in real environments the planar model works extremely well even for non-planar surfaces and is robust enough for reliable range measurements. Since the applied algorithm can filter the entire frame, the algorithm is quite efficient and effective for TOF based applications.

9 CONCLUSIONS

The use of Time-of-flight (TOF) cameras is increasing in various applicati6ns ranging from medical to automotive. TOF manufacturer companies are progressing rapidly to increase the resolution and range of the camera. However, the range pixel reliability has not been addressed effectively in the literature. The use of radiometric model for all the available measurement parameters helps in formulating a robust range reliability criterion that is independent of scene reflectivity and will make a substantial difference to how range pixel reliability is classified.

ACKNOWLEDGEMENTS

This work is supported by Seeing Machines Ltd. and the Commonwealth of Australia, through the Cooperative Research Centre for Advanced Automotive Technology.

REFERENCES

Alldrin, N., Zickler, T., and Kriegman, D. (2008). Photometric stereo with non-parametric and spatially-varying reflectance. In *Proc. IEEE Conference on Computer Vision and Pattern Recognition CVPR 2008*, pages 1–8.

Bodek, A. (1974). The mean of several quotients of two measured variables. SLAC Technical Note.

Bonny, J.-M., Renou, J.-P., and Zanca, M. (1996). Optimal measurement of magnitude and phase from MR data. *Journal of Magnetic of Resonance, Series B*, 113(2):136–144.

Büttgen, B., Lustenberger, F., and Seitz, P. (2006). Demodulation pixel based on static drift fields. *IEEE Trans. Electron Devices*, 53(11):2741–2747.

Cook, R. L. and Torrance, K. E. (1982). A reflectance model for computer graphics. *ACM. Trans. on Graphics*, 1(1):7–24.

Fardi, B., Dousa, J., Wanielik, G., Elias, B., and Barke, A. (2006). Obstacle detection and pedestrian recognition using a 3D PMD camera. In *Proc. IEEE Intell. Vehicles Symp.*, pages 225–230.

Foley, J. D., Da, A. v., Feiner, S. K., and Hughes, J. F. (1997). *Computer Graphics: Principles and Practices*. Addisin-Wesley Publishing Company, Inc.

Forsyth, D. A. and Ponce, J. (2003). *Computer Vision: A Modern Approach*. Prentice Hall.

Horn, B. (1986). *Robot Vision*. The MIT Press.

Horn, B. K. P. (1977). Image intensity understanding. *Artificial Intelligence*, 8(2):201–231.

Kahlmann, T., Remondino, F., and Guillaume, S. (2007). Range imaging technology: new developments and applications for people identification and tracking. In *Proc. SPIE-IS&T Electronic Imaging*, volume 6491, San Jose, CA, USA.

Kahlmann, T., Remondino, F., and Ingensand, H. (2006). Calibration for increased accuracy of the range imaging camera SwissRanger. In *Proc. International Archives of Photgrammetry, Remote Sensing and Spatial Information Sciences, ISPRS Commission V Symposium*, volume XXXVI, pages 136–141.

Klasing, K., Althoff, D.,Wollherr, D., and Buss, M. 2009 Comparison of surface normal estimation methods for range sensing applications. In *Proc. IEEE International Conference on Robotics and Automation ICRA* 09, pages 32063211.

Kuhnert, K.-D. and Stommel, M. (2006). Fusion of stereo-camera and PMD-camera data for real-time suited precise 3D environment reconstruction. In *Proc. IEEE/RSJ Int. Conf. Intell. Robot. Systs.*

Lange, R. and Seitz, P. (2001). Solid-state time-of-flight range camera. *IEEE J. Quantum Electron.*, 37:390–397.

Lindner, M. and Kolb, A. (2006). Lateral and depth calibration of PMD-distance sensors. In *Proc. International Symposium on Visual Computing (ISVC06)*, volume 2, pages 524–533. Springer.

Lindner, M. and Kolb, A. (2007). Calibration of the intensity-related distance error of the PMD TOF-camera. In *Proc. SPIE, Intelligent Robots and Computer Vision XXV: Algorithms, Techniques, and Active Vision*, volume 6764.

Luan, X. (2001). *Experimental Investigation of Photonic Mixer Device and Development of TOF 3D Ranging Systems Based on PMD Technology*. PhD thesis, Department of Electrical Engineering and Computer Science at University Of Siegen.

Ma, Y., Soatto, S., Košecká, J., and Sastry, S. S. (2003). *An Inviation to 3-D Vision: From Images to Geomtric Models*. Springer Verlag. Ch. 2.

Meier, E. and Ade, F. (1997). Tracking cars in range image sequnces. In *Proc. IEEE Int. Conf. Intell. Trans. Systs.*, pages 105–110.

Moller, T., Kraft, H., Frey, J., Albrecht, M., and Lange, R. (2005). Robust 3D measurement with PMD sensors. In *Proc. 1st Range Imaging Research Day*, ETH Zurich, Zurich, Switzerland.

Mufti, F. and Mahony, R. (2009). Statistical analysis of measurement processes for time-of-flight cameras. In *Proc. SPIE Videometrics, Range Imaging, and Applications X*, volume 7447-21.

PMD (2002). PMD tech. http://www.pmdtec.com.

Pulli, K. and Pietikainen, M. (1993). Range image segmentation based on decomposition of surface normals. In *Proc. 8th Scandinavian Conference on Image Analysis*, pages 893–899.

Radmer, J., Fuste, P. M., Schmidt, H., and Kruger, J. (2008). Incident light related distance error study and calibration of the PMD-range imaging camera. In *IEEE Conf.Computer Vision and Pattern Recognition Workshops*, 2008, pages 16.

Sillion, F. X. and Puech, C. (1994). *Radiosity and Global Illumination*. Morgan Kaufmann.

Ye, C. and Hegde, G.-P. M. (2009). Robust edge extraction for SwissRanger SR-3000 range images. In *Proc. IEEE International Conference on Robotics and Automation ICRA09*, pages 24372442.

Zhang, R., Tsai, P.-S., Cryer, J., and Shah, M. (1999). Shape from shading: A survey. *IEEE Trans. Pattern Anal. Mach. Intell.*, 25(11):1416–1421.

Zheng, Q. and Chellappa, R. (1991). Estimation of illumination direction, albedo, and shape from shading. *IEEE Trans. Pattern Anal. Mach. Intell.*, 13(7):680–702.

Zhou, S., Aggarwal, G., Chellappa, R., and Jacobs, D. (2007). Appearance characterization of linear lambertian objects, generalized photometric stereo, and illumination-invariant face recognition. *IEEE Trans. Pattern Anal. Mach. Intell.*, 29(2):230–245.